Hydroxyapatite based hybrid dental materials with controlled porosity and improved tribological and mechanical properties

S. Vargas[1], M. Estevez[1], A. Hernandez[1], J. C. Laiz[1], W. Brostow*[2], H. E. Hagg Lobland[2] and J. R. Rodriguez[1]

Hybrid dental materials were designed with controlled porosity and improved tribological and mechanical properties. These materials are based on hydroxyapatite (HAp) and reinforced with two different types of ceramic particles, alumina and silica, to support the high stresses and the continuous scratching produced during mastication. The agglutinant phase is an alkyd polyester polyurethane with high abrasion resistance that adheres well to surfaces containing OH groups. Porosity of the materials was controlled using sodium acetate powder of specified particle size as a pore former, thereby providing the materials with a morphology that resembles real teeth. The composition, structure and morphology were evaluated through several analytical techniques; results of scanning electron microscopy, dynamic light scattering, Fourier transform infrared spectroscopy, X-ray diffraction, induced coupled plasma optical emission spectroscopy and densitometry are reported. The ceramic powders incorporated (HAp, alumina and silica) were a combination of micro- and nanoscale particles; this use of different sized particles improved the packing and consequently the mechanical and tribological properties of the dental materials. Tribological features are explained from results of microscratch testing and abrasion resistance. The elastic modulus from mechanical testing is compared for the entire set of hybrid dental composites developed.

Keywords: Tribological properties, Scratching, Nanohybrids, Hydroxyapatite, Alumina, Silica

Introduction

Dental obturation materials are perhaps the simplest biomaterials introduced into the human body because there are relatively few properties to control: mechanical and tribological properties sufficient to support the stresses, scratching and abrasion processes suffered during mastication and brushing along with good adhesion to the substrate to avoid microfiltration. However, it is known that the mastication process produces fatigue in obturation materials leading to premature wear and eventual performance failure.[1–4] Moreover, the mechanical stresses have negative effects on tribological properties resulting in cracks and fissures that can damage the dental enamel.[5–7] Tribological experiments are commonly used to compare the performance of obturation materials, which are subjected to intense shear and compression stresses and continuous scratching and wearing processes.[8–11] Both the natural teeth and the repairing synthetic material must have the capacity to support these intensive conditions.[12] Currently, there is an additional demand for more than just simple obturation materials; it is desirable to have dental obturations that permit vascularisation and foster new tissue growth.[13,14]

There is a considerably long list of different types of biomaterials designed as implants and prostheses to replace or fix bone and teeth.[15–20] These biomaterials must fulfil several tough requirements, including bioacceptance (eliciting a good host response), relatively high mechanical and tribological properties (to support stresses inherent at the implant site), good hydrolytic stability (to maintain chemical integrity), appropriate morphology (allowing vascularisation and the support of cellular activity in interconnected pores) and good adhesion to the substrate, which for dental materials is dentin (to prevent microfiltrations).[21–24] These conditions demand a matching of properties (chemical and morphological) between the biomaterials and the real bone or teeth in order to support tissue regeneration.[25–28]

While there are a variety of obturation materials in commercial use and in development, there still exists a high demand for aesthetic and highly durable dental

[1]Centro de Fisica Aplicada y Tecnología Avanzada (CFATA), Universidad Nacional Autonoma de Mexico, Campus Juriquilla, Queretaro, CP 76230, Mexico
[2]Laboratory of Advanced Polymers & Optimized Materials (LAPOM), Department of Materials Science & Engineering, University of North Texas, 1150 Union Circle 305310, Denton, TX 76203-5017, USA

*Corresponding author, email wbrostow@yahoo.com

Received 5 January 2012; accepted 26 August 2012
DOI 10.1179/1433075X12Y.0000000063

materials. The designs of these materials are generally based on the dentin chemistry and morphology: a structured composite made of organic (collagen, etc.) and mineral [hydroxyapatite (HAp)] constituents with specific morphology. It is known that when ceramic particles are added to a polymeric matrix, the mechanical properties of the composite are generally improved;[29–32] in the present study, two different types of ceramic particles (silica and alumina) of different sizes (nano- and microparticles) were added to fulfil the tough requirements imposed on the HAp containing resin obturation material. The mechanical and tribological properties of the final hybrid material depend strongly on the hardness and size of the ceramic particles. The surface chemistry of the ceramic particles determines their compatibility with the resin and their potential for reactivity with the curing agent to form a network in the material, thereby improving its performance.[33,34]

Porous biomaterials have attained special relevance because, with them, it is possible to mimic the morphology of bones or teeth in the fabrication of prostheses and implants.[35–38] The porous structure of the biomaterials synthesised here was achieved using sodium acetate powder of a specified size as pore forming agent. The other components of our dental hybrids are the polymer resin, a polyisocyanate curing agent, HAp, silica and alumina. Once the polymer has been cured, i.e. when the chemical reaction between the resin and the polyisocyanate is complete, the biomaterial reaches dimensional stability and the pore forming agent can be removed, leaving an interconnected porous structure.

We synthesised and tested a series of polymer + ceramic hybrids, comparing their performance. These obturation materials were prepared using an alkyd based two-component polyurethane (PU) as agglutinant. This polymer has good mechanical properties, high agglutination capacity, good adhesion to dentin, high abrasion resistance and good tailorability. In addition, it is possible to vary the stiffness of the material through a wide range by mixing, in appropriate concentrations, polyester and polyether resins to produce PU resins with rigidity, semirigidity or flexibility.[39,40]

Acrylic based PUs were also prepared and tested, but the presence of remaining unreacted cyano groups was detected;[41] consequently, those materials were not considered appropriate for dental applications. Because the polyisocyanate reacts with all OH groups present in the alkyd system, we are assured good adhesion between the substrate (dentin) and the obturation material (thereby reducing the risk of microfiltration in the interface). Synthesis and characterisation of the materials are described below.

Experimental

Materials

The samples were prepared using synthetic HAp prepared as reported elsewhere;[42] this was ground in an agate mortar to a nominal size of 1·9 μm. The polymeric agglutinant was a two-component alkyd PU: the aliphatic alkyd hydroxylated polyester resin (Reichhold Mexico) was mixed with an aliphatic polyisocyanate (Bayer, Germany) in a proportion of 4 : 1 (v/v). Ceramic particles of different sizes were used: alumina microparticles (Cabot, USA) with 2·7 μm average diameter and silica nanoparticles (Degussa, Germany) with 16 nm diameter. The pore formation agent was sodium acetate trihydrated (Aldrich, USA) ground at 150 μm; 21 g of the sodium acetate (Table 1) was added to produce, in the final material, a pore volume fraction of ~55 wt-%.

Sample preparation

For all samples, the amounts of polyester resin, the polyisocyanate and the sodium acetate were kept constant at 10, 2·5 and 21 g respectively (Table 1). The resin was mixed with the sodium acetate (150 μm particles) with strong agitation until a homogeneous dispersion was obtained; 2·5 g of polyisocyanate was added to this mixture to full incorporation. Finally, different amounts of ceramic particles were added slowly and with strong agitation to obtain a homogeneous final material. The particles were added following an order according to their sizes: first the alumina microparticles (2·7 μm average diameter), followed by HAp (1·9 μm diameter) and finally the silica nanoparticles (16 nm diameter); the ceramic particles were added to reach saturation with respect to resin, and these concentrations are reported in Table 1. All samples were kept for 48 h at room conditions to allow finishing the curing reaction. Seven samples of each formulation and different shapes were prepared: discs 2 cm in diameter and 0·5 cm in thickness for abrasion and tribological analysis and cylinders 1·0 cm in diameter and 2·0 cm in length for mechanical testing. After the curing time, all samples were placed in distilled water with mild agitation during 3 days in order to remove the sodium acetate; fresh distilled water was changed five times per day.

Characterisation

The crystallographic characterisation of the synthetic HAp was conducted by X-ray diffraction (XRD) using a Rigaku machine model Miniflex with a radiation source of 0·154 nm (Cu K_α line) and the angle 2Q was varied from 5 to 80° at a scan of 1° min^{-1}. The identification of

Table 1 Chemical compositions of samples studied

Sample	Resin/g	CH_3COONa/g	Isocyanate/g	HAp/g	Al_2O_3/g	S_iO_2/g	Pore size/μm
H	10	21	2·5	5*	0	0	161 ± 101
A	10	21	2·5	0	5*	0	100 ± 64
S	10	21	2·5	0	0	5*	114 ± 72
A5S5	10	21	2·5	0	2·5	2·5	102 ± 38
A7S3	10	21	2·5	0	3·5	1·5	115 ± 64

*Saturation concentration.

the crystalline phases was performed according to the MDI JADE 5·0 software.

Composition

The densities were determined weighting the samples in an analytical balance with a resolution of 10^{-5} g and measuring the discs sizes with a micrometre with resolution of 0·001 mm and an accuracy of $\pm$0·001 mm. The synthetic HAp was also characterised by determining the stoichiometric Ca/P ratio using the induced coupled plasma optical emission spectroscopy using a Thermo Scientific apparatus model iCAP 6000 DUO. The samples were prepared following a procedure described elsewhere.[14] The particle size analysis of the ceramic particles was performed in a dynamic light scattering apparatus Brookhaven Instruments Corp. model BI-APD equipped with an He–Ne laser at 632·8 nm and a digital correlator.

Spectroscopy

The Fourier transform infrared (FTIR) analysis was performed in a Bruker model Alpha-T spectrometer equipped with diffuse reflectance and attenuated total reflectance. The m-Raman analysis was performed in a Bruker Senterra apparatus with a resolution of 9–15 cm^{-1} equipped with a laser of 785 nm, while the integration time was 15 s. The determination of the unreacted cyano groups present in the samples was obtained according to the ASTM D2572-87 standard. This norm provides the concentration of the unreacted cyano groups in PU by the titration method; this procedure was repeated five times. A sample was precisely weighted and placed in a 250 mL Erlenmeyer bottle. Toluene (25 mL) was added, and the bottle was caped hermetically and shaken; 25 mL of a solution 0·1M di-*n*-butilamina in toluene was added and agitated during 30 min caped. Isopropanol (100 mL) was added together with five drops of blue bromophenol and titrated with 0·1 N of hydrochloric acid to obtain a yellow colour. The content of NCO groups was determined using the equation

$$\mathrm{NCO}\,(\%) = \left[\frac{(B-V)(M)(0{\cdot}0420)}{W}\right] \times 100 \qquad (1)$$

where B are the millilitres of HCl required for titration of the reference, V are the millilitres of HCl required for titration of the sample, M is the molarity of HCl (0·1000), 0·0420 is the gram milliequivalent of the cyano group and W is the weight of the sample.

Microscopy

Scanning electron microscopy (SEM) images were obtained using a JEOL JSM-6060 LV at 20 kV in secondary electron mode at several magnifications.

Mechanics

The mechanical tests were performed in an Adamel Lhomargy machine model DY.22 in a compression mode according to the norm ASTM D-695-02a using a compression rate of 1·3 mm min^{-1}.

Tribology: scratch resistance

The scratching analysis was performed using a micro-scratch tester CSM Instruments (Peseux, Switzerland), where the indenter was a Rockwell diamond tip with a 200 μm radius. Constant load tests consisting of 15 scratches along the same groove (referred to as sliding wear) were conducted (*see* Refs. 43–45 for more about sliding wear procedure and theory). The scratch length was 5·0 mm, and scratching speed was 1 mm min^{-1}; samples were tested in triplicate at each of three different loads (5·0, 10·0 and 15·0 N). For each scratch, the penetration depth R_p, or instantaneous depth of penetration by the indenter, was measured and recorded. Because of the viscoelastic nature of polymers, there is a recovery or healing of the scratch groove.[46–50] The scratch remains but with a shallower depth called the residual or the healing depth R_h. The extent of healing depends on the load and the properties of the material.[43,45,46,50] The percentage of recovery (healing) $R_{\%}$ is defined as[43,46,51]

$$R_{\%} = \left(1 - \frac{R_h}{R_p}\right) \times 100 \qquad (2)$$

An interesting phenomenon referred to as strain hardening has been observed in sliding wear tests.[45,51] Although the first few passes of the indenter result in successively deeper groove, beyond that, a hardening occurs and subsequent scratches do not lead to deepening of the scratch groove. In the course of 15 successive scratches, the value of the penetration and residual depths plateaus; therefore, the values from the 15th pass are used to characterise specimen behaviour.

Tribology: wear resistance

The wearing resistance was determined according to the norm ASTM standard D-1242 95a (Taber method).[52] The sample was sanded using a F-400 Fandeli sandpaper mounted on a steel plate rotating at 90 rev min^{-1} in dry conditions and loaded with a weight of 20 g; every 20 s, the scratched sample was cleaned using a dry soft cloth wipe to remove the dust and weighted with an accuracy of $\pm 1 \times 10^{-5}$ g; the sand paper was also cleaned with a soft brush. The samples were discs 2 cm in diameter and 0·5 cm thick. Five experiments of each sample were performed, all at room temperature.

Results and discussion

Particle size of HAp, silica and alumina was confirmed by the dynamic light scattering technique. The following results were obtained: 16$\pm$1 nm for the silica nanoparticles, 2·7$\pm$1·5 μm for alumina and 1·9$\pm$1·5 μm for HAp. The HAp was further analysed by XRD. X-ray diffraction patterns for the synthetic HAp treated at 700°C during 12 h (Fig. 1) and at 900°C during 15 h (not shown) were obtained. For the sample treated at 700°C, the diffractogram shows only reflections corresponding to HAp: at this temperature, this is the only phase present, and the size of the crystallite as determined using the Scherer equation is 11 nm. For HAp treated at 900°C, additional small reflections appear, suggesting that another crystalline phase is emerging: tricalcium phosphate [$Ca_3(PO_4)_2$]. When the HAp is treated at 900°C during 15 h, the HAp starts a decomposition process producing tricalcium phosphate. For the preparation of all samples, only HAp treated at 700°C was used. The XRD patterns for the alumina particles (not shown) indicate that the alumina was in α phase. The stoichiometry of the synthetic HAp was obtained from a determination of the Ca/P ratio using the induced coupled plasma technique, resulting in a value of 1·679, which is very close to the stoichiometric value (1·667).

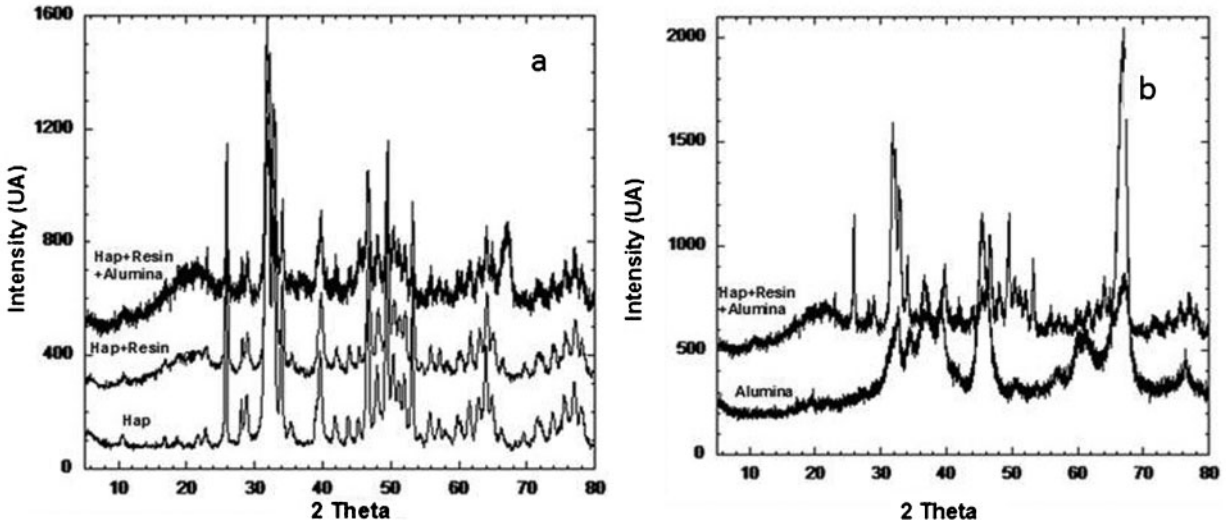

1 X-ray diffraction pattern for *a* synthetic HAp (thermally treated at 700°C during 12 h), HAp+resin and HAp+resin+alumina and *b* alumina and HAp+resin+alumina

Fourier transform infrared spectra have confirmed the composition of the commercial and synthetic (700°C 12 h) HAp samples.[15] Figure 2 shows a typical FTIR spectrum of one of the final prepared biomaterials (sample A, described in Table 1; for brevity, the spectra for others are not shown). A comparison between the spectrum of the commercial and the synthetic HAp shows that these materials are chemically identical. The spectrum reported in Fig. 2 shows a band at 705 cm^{-1} corresponding to the Al–O stretching vibration group, while the band at 800 cm^{-1} corresponds to the stretching deformation of the Al–O–Al group; the band at 1070 cm^{-1} is assigned to the symmetric stretching vibration of the Al–CH_3 group. Similarly, the spectra for the other prepared specimens show the expected bands corresponding to the chemical composition. It is important to mention that bands corresponding to isocyanate (2250–2300 cm^{-1}) were not found in any of the final prepared materials, meaning that the isocyanate has reacted totally during the curing reaction. This is further confirmed by the results of the determination of unreacted NCO groups by the titration method in conjunction with equation (1). The average NCO concentration was 0·084 ppm; this value is lower than the maximum allowed value of 0·2 ppm.

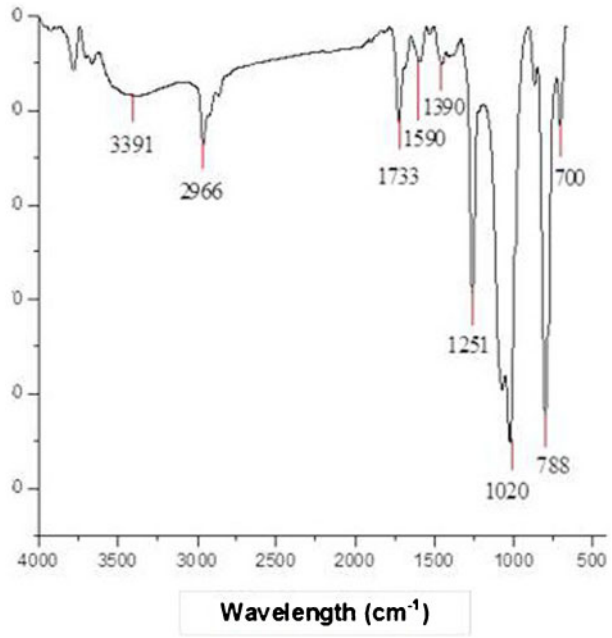

2 Typical FTIR spectrum of final biomaterial containing only alumina

It is known that a pore volume fraction between 50 and 60% is required to allow the vascularisation of the material; at this pore volume fraction, the pores are percolated. We adjusted the concentration of the ceramic particles and the pore former agent to produce materials with a pore volume fraction ~55%. The pore sizes of our hybrids are reported in Table 1. It is noticeable that the pore sizes are in accordance with the size of the sodium acetate particles (150 μm).

Mechanical strength of the dental hybrids was evaluated by determination of the Young's modulus; results are shown in Fig. 3. Here, it is possible to see that, even when the materials have a high pore volume fraction (55%), the values of the Young's moduli are relatively high; the alkyd PU is responsible for these values. When a combination of different sized ceramic particles is added to a polymeric resin, the smaller

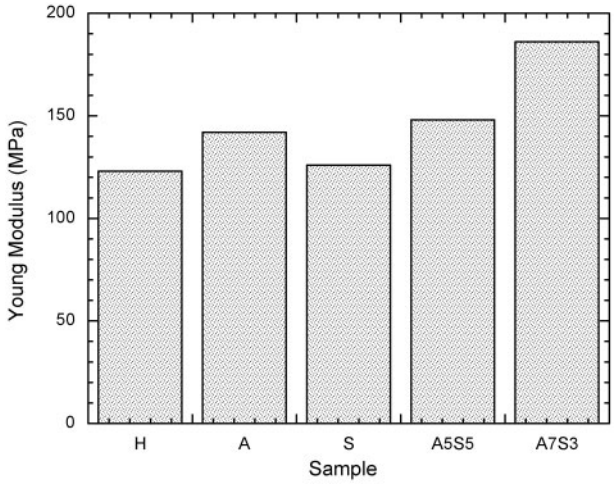

3 Young's modulus

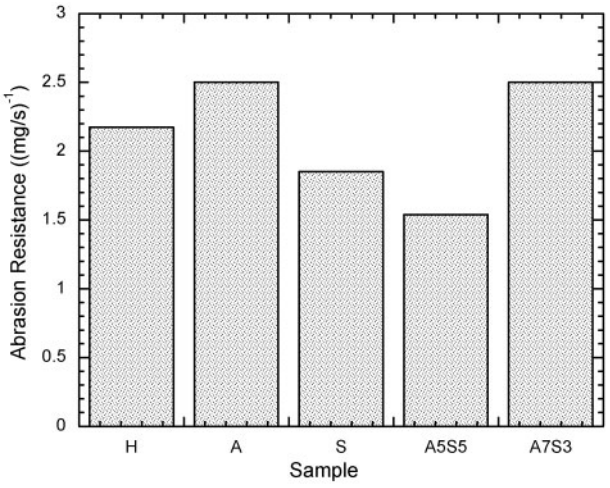

4 Abrasion resistance

particles fill the interstitial spaces left by the large particles, densifying the material and improving the mechanical properties. In Fig. 3, we observe that sample A7S3 containing 70% alumina and 30% silica (Table 1) has the highest Young's modulus (186 MPa), while the sample with only HAp added has the lowest value (123 MPa): the hardness of HAp particles is lower with respect to alumina or silica.

From the abrasion experiments, we determined that for all samples, the weight is lost linearly with time. Therefore, we evaluate the rate of weight lost, which is the slope of the weight versus time curves. Abrasion resistance is defined as the inverse of the weight loss rate; these values are reported in Fig. 4. As we saw in the results of mechanical testing, the best performance is for samples containing alumina. We conclude that the hardness of alumina increases significantly the abrasion resistance.

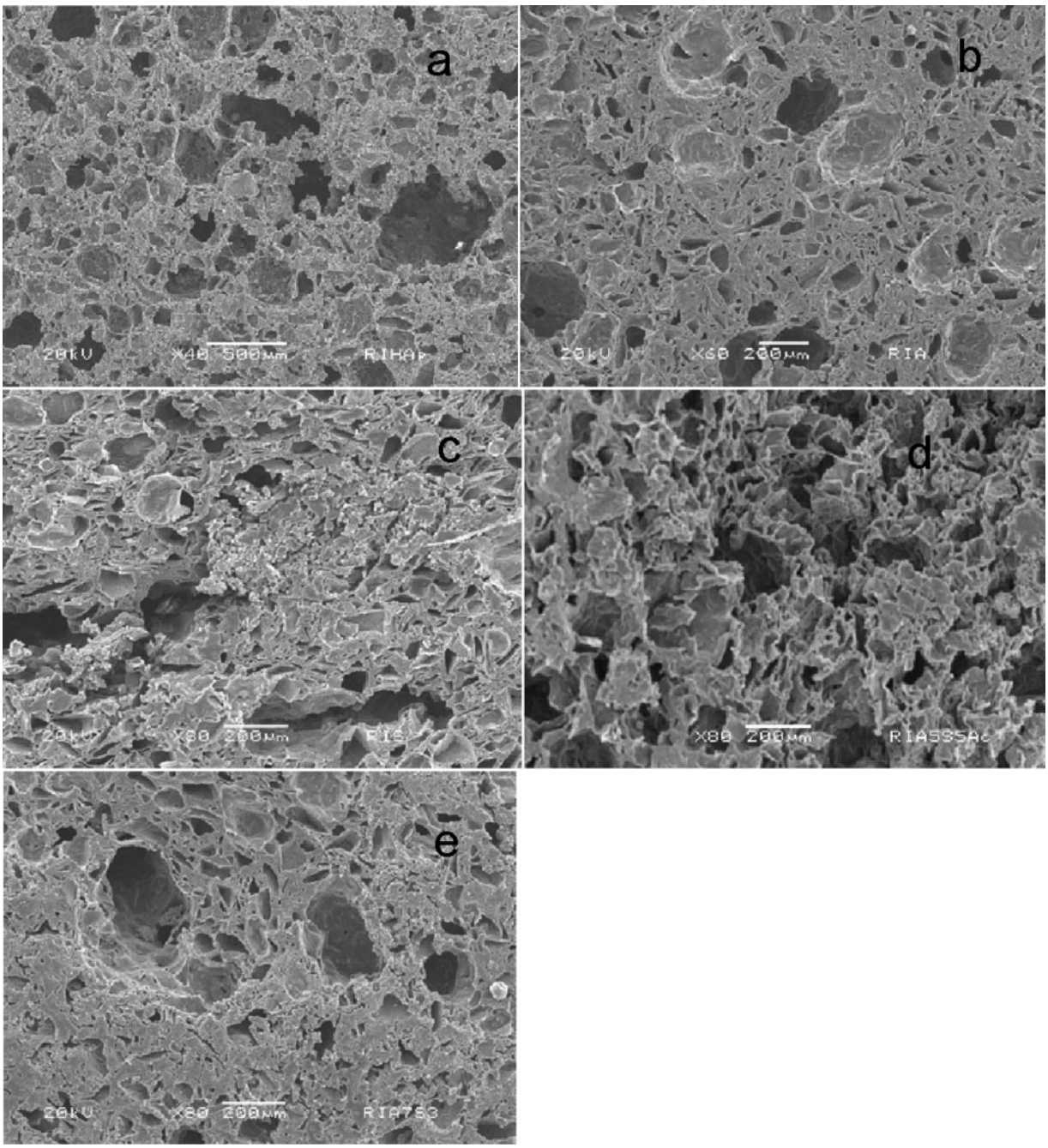

a H; *b* A; *c* S; *d* A5S5; *e* A7S3

5 Images (SEM) of samples with different chemical compositions

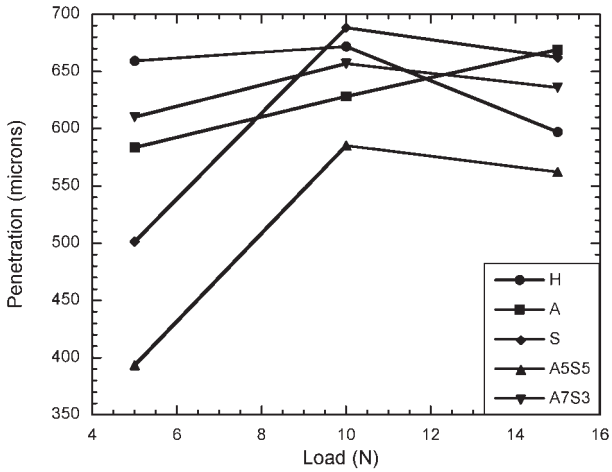

6 Penetration depth as function of load

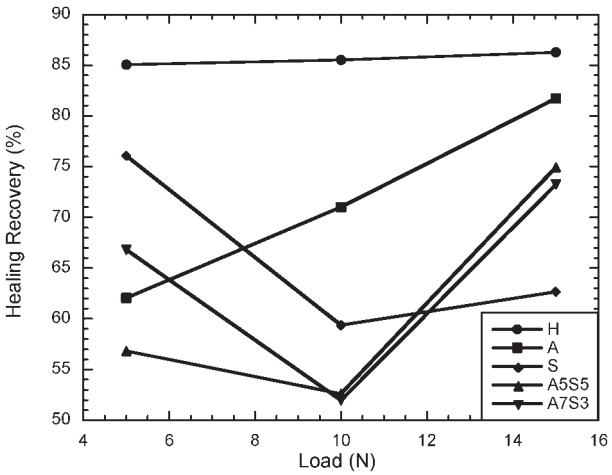

8 Percentage healing recovery as function of load

We can see the morphology of our samples as shown in SEM images of Fig. 5. From these and additional images, the average pore size (with standard deviation, as reported in Table 1) for each specimen was determined. The results agree with expectations based on the pore former used.

The results of the tribological analysis via scratch testing are summarised in Figs. 6–8. As mentioned, R_p is a measure of the instantaneous scratch depth. In Fig. 6, penetration depth is reported as a function of the applied load. We shall discuss these results more in detail after looking at residual depths in Fig. 7.

Consider the simpler cases first. For the material containing either only HAp or only alumina but not silica, we find that the final or residual depths are shallower at higher loads. Since we are dealing with porous and also rigid materials, higher loads cause a decrease in the pore sizes, thus increased resistance of materials against scratching.

The behaviour of the other three materials is different. They all contain silica nanopowder, and they all exhibit maxima on the depth (whether penetration or recovery) versus load diagrams. Phenomena that play a role here are related to the fact that, at given weight percentage of the filler, silica with particles in the nanometre size range has a much larger surface area than fillers with sizes in the micrometre range. Thus, many OH groups on the silica surface can react with the polyisocyanate. This leaves less polyisocyanate molecules available to react with the resin molecules, reducing the crosslinking between the polyisocyanate and the resin, thus weakening the network. Higher depths in the scratch resistance determination at lower loads are the result. At higher loads, the effect of reduction in the volume fraction of pores resulting in more resistance against scratching begins to dominate; hence, the depths decrease. The highest value of the residual depth R_h at 15 N among all nanohybrids is seen for material S, which does not contain alumina or HAp, only silica (Table 1).

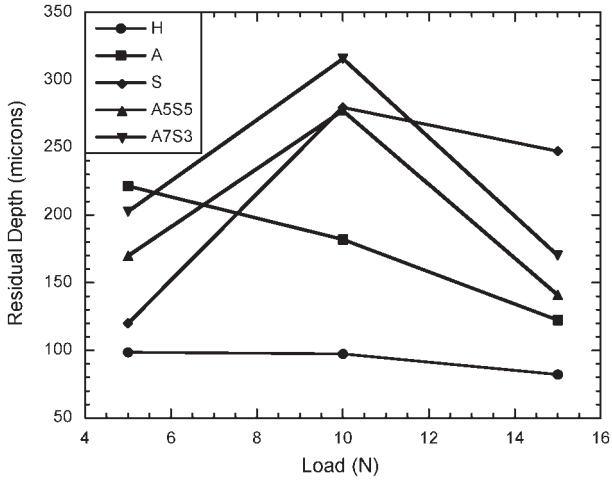

7 Residual depth as function of load

The percentage of the recovery, called healing recovery, is defined by equation (2) and reported in Fig. 8. The sample containing only HAp shows a high percentage of recovery (85%) independent of the load, followed by the sample A, which contains alumina only and reaches 80% of recovery at 15 N. The other three materials all contain silica and exhibit minima on the recovery versus load diagrams, a reflection of the behaviour seen in Figs. 6 and 7 and discussed above.

A survey of results

The results above describe several important behaviours in the characterisation of potential obturation materials. As indicated at the start, there is room for improvement in obturation materials as the chemical environment of the mouth, the mechanical and tribological stresses of mastication and the delicacy of biological incorporation within the existing tooth infrastructure all demand particular performance properties. The specimens in the present study differ from other obturation materials, including those we have reported on previously, in several aspects. For instance, while we have worked with PU compounds containing silica and alumina fillers before,[15] the present system is a two-component solvent based aliphatic PU cured with poly isocyanate, whereas elsewhere, we describe a water based mono component PU cured with a blocked poly isocyanate.[15] In the latter, pores are formed by breaking of the blocking structure of the isocyanate, while in the former, ammonium acetate is used as a pore former. Also in the present two-component system, we have used thermal treatment to effectively produce pores of different sizes.

The overall mechanical and tribological performance of the materials described herein is somewhat less than that of the specimens prepared from the water based PU

system studied earlier.[15] However, this investigation confirms the positive synergistic effect of incorporating different sized particles of alumina and silica on Young's modulus and wear resistance. However, beneficial effects of the reinforcement are by no means automatic, as seen in the discussion of scratch testing results above. The benefits of the multiscaled filler approach are not limited to one type of polymer matrix. Therefore, we are now poised to make further advancements in development of obturation materials that can meet the high demands of the next generation of such materials.

Acknowledgements

The authors are in debt to Gerardo Fonseca for the mechanical analysis and to Alicia del Real for the SEM images.

References

1. J. N. Uy, J. C. L. Neo and S. H. Chan: *J. Prosthet. Dent.*, 2010, **104**, 318–324.
2. D. Arola, D. Bajaj, J. Ivancik, H. Majd and D. Zhang: *Int. J. Fatigue*, 2010, **32**, 1400–1412.
3. J. M. Anderson: in 'Foundations of regenerative medicine', (ed. A. Atala *et al.*), 693–716; 2011, San Diego, CA, Academic Press.
4. D. Shrestha, X. Wei, W.-C. Wu and J.-Q. Ling: *J. Dent. Sci.*, 2010, **5**, 47–52.
5. Y.-R. Jeng, T. T. Lin and D.-B. Shieh: *J. Biomech.*, 2009, **42**, 2249–2254.
6. J. A. Arsecularatne and M. Hoffman: *J. Mech. Behav. Biomed. Mater.*, 2010, **3**, 347–356.
7. R. S. Austin, J. M. Rodriguez, S. Dunne, R. Moazzez and D. W. Bartlett: *J. Dent.*, 2010, **38**, 782–787.
8. A. de la Isla, W. Brostow, B. Bujard, M. Estevez, R. Rodriguez, S. Vargas and V. M. Castaño: *Mater. Res. Innov.*, 2003, **7**, 110.
9. M. Estevez, S. Vargas, A. de la Isla, W. Brostow, V. M. Castaño and J. R. Rodriguez: *Mater. Res. Innov.*, 2005, **9**, 61.
10. B. Bilyeu, W. Brostow, L. Chudej, M. Estevez, H. E. Hagg Lobland, J. R. Rodriguez and S. Vargas: *Mater. Res. Innov.*, 2007, **11**, 181.
11. M. Esteves-Oliveira, C. Pasaporti, N. Heussen, C. P. Eduardo, F. Lampert and C. Apel: *J. Dent.*, 2011, **39**, 604–611.
12. H. Yu, F. J. Wegehaupt, A. Wiegand, M. Roos, T. Attin and W. Buchalla: *J. Dent.*, 2009, **37**, 913–922.
13. W. Brostow, M. Estevez, H. E. Hagg Lobland, L. Hoang, J. R. Rodriguez and S. Vargas: *J. Mater. Res.*, 2008, **23**, 1587.
14. W. Brostow, J. R. Rodriguez, M. Estevez, S. Vargas, H. E. Hagg Lobland and J. A. Guerra: *J. Nanosci. Nanotechnol.*, 2012, 12, to be published.
15. A. Saenz, W. Brostow, E. Rivera and V. M. Castaño: *J. Mater. Educ.*, 1999, **21**, 267.
16. S. V. Dorozhkin: *Biomaterials*, 2010, **31**, 1465–1485.
17. F. B. Teixeira, E. C. N. Teixeira, J. Y. Thompson and M. Trope: *J. Am. Dent. Assoc.*, 2004, **135**, 646–652.
18. D. Bozukova, C. Pagnoulle, R. Jérôme and C. Jérôme: *Mater. Sci. Eng. R*, 2010, **R69**, 63–83.
19. Y. Oxida, C. B. Sellers, K. Mirza and F. Farzin-Nia: *Mater. Sci. Eng. C*, 2005, **C25**, 343–348.
20. E. K. Tschegg, R. A. Lindtner, V. Doblhoff-Dier, S. E. Stanzl-Tschegg, G. Holzlechner, C. Castellani, T. Imwinkelried and A. Weinberg: *J. Mech. Behav. Biomed. Mater.*, 2011, **4**, 766–775.
21. S. H. Teoh: *Int. J. Fatigue*, 2000, **22**, 825–837.
22. S.-L. Liang, W. D. Cook, G. Thouas and Q.-Z. Chen: *Biomaterials*, 2010, **31**, 8516–8529.
23. A. Ulrich, N. Ott, A. Tournier-Fillon, N. Homazava and P. Schmutz: *Spectrochim. Acta B*, 2011, **66B**, 536–545.
24. J. Yang and H.-J. Xiang: *J. Biomech.*, 2007, **40**, 2377–2385.
25. L. Lin, M. Y.-H. Chen, D. Ricucci and P. A. Rosenberg: *J. Endodont.*, 2010, **36**, 618–625.
26. T. Hoshi, T. Sawaguchi, R. Matsuno, T. Konno, M. Takai and K. Ishihara: *J. Supercrit. Fluids*, 2008, **44**, 391–399.
27. R. J. Kane, G. L. Converse and R. K. Roeder: *J. Mech. Behav. Biomed. Mater.*, 2008 **1**, 261–268.
28. S. Kapfer, S. Sporer, S. T. Hyde, K. Mecke and G. E. Schroeder-Turk: *Biophys. J.*, 2010, **98**, 571a.
29. A. T. Hara, C. González-Cabezas, J. Creeth, M. Parmar, G. J. Eckert and D. T. Zero: *J. Dent.*, 2009, **37**, 781–785.
30. G. Bogen and S. Kuttler: *J. Endodont.*, 2009, **35**, 777–790.
31. J. Chevalier and L. Gremillard: *J. Eur. Ceram. Soc.*, 2009, **29**, 1245–1255.
32. M. Kes, H. Polat, S. Kelesoglu, M. Polat and G. Aksoy: *J. Eur. Ceram. Soc.*, 2009, **29**, 2959–2967.
33. C. Kaya, F. Kaya, E. G. Butler, A. R. Boccaccini and K. K. Chawla: *J. Eur. Ceram. Soc.*, 2009, **29**, 1631–1639.
34. H. Ghomi, M. Jaberzadeh and M. H. Fathi: *J. Alloys Compd*, 2011, **509**, L63–L68.
35. M. C. Popescu, C. Vasile, D. Macocinschi, M. Lungu and O. Craciunescu: *Int. J. Biol. Macromol.*, 2010, **47**, 646–653.
36. M. Nakai, M. Niinomi and D. Ishii: *J. Mech. Behav. Biomed. Mater.*, 2011, **4**, 1206–1218.
37. J.-Y. Sun and J. Tong: *J. Bionic Eng.*, 2007, **4**, 11–17.
38. R. Diaz, E. Rivera-Muñoz, W. Brostow and V. M. Castaño: *J. Mater. Sci. Med.*, 2001, **12**, 305.
39. J. Zhang and C. P. Hu: *Eur. Polym. J.*, 2008, **44**, 3708–3714.
40. J. M. Herrera-Alonso, E. Marand, J. C. Little and S. S. Cox: *J. Membr. Sci.*, 2009, **337**, 208–214.
41. C. E. Fernández, M. Bermúdez, R. M. Versteegen, E. W. Meijer, G. J. Vancso and S. Muñoz-Guerra: *Eur. Polym. J.*, 2010, **46**, 2089–2098.
42. I. Mobasherpour, M. Soulati Heshajin, A. Kazemzadeh and M. Zakeri: *J. Alloys Compd*, 2007, **430**, 330–333.
43. W. Brostow, J.-L. Deborde, M. Jaklewicz and P. Olszynski: *J. Mater. Educ.*, 2003, **25**, 119.
44. W. Brostow, J. A. Hinze and R. Simões: *J. Mater. Res.*, 2004, **19**, 851.
45. W. Brostow, H. E. Hagg Lobland and M. Narkis: *J. Mater. Res.*, 2006, **21**, 2422.
46. W. Brostow, B. Bujard, P. E. Cassidy, H. E. Hagg and P. E. Montemartini: *Mater. Res. Innov.*, 2002, **6**, 7.
47. W. Brostow and R. Simões: *J. Mater. Educ.*, 2005, **27**, 19.
48. M. Estevez, S. Vargas, H. E. Hagg Lobland, A. de la Isla, W. Brostow and J. R. Rodriguez: *Mater. Res. Innov.*, 2006, **10**, 411.
49. W. Brostow, W. Chonkaew, T. Datashvili and K. P. Menard: *J. Nanosci. Nanotechnol.*, 2008, **8**, 1916.
50. W. Brostow, V. Kovacevic, D. Vrsaljko and J. Whitworth: *J. Mater. Educ.*, 2010, **32**, 273.
51. W. Brostow, G. Damarla, J. Howe and D. Pietkiewicz: *e-Polymers*, 2004, 025.
52. M. Vorbau, L. Hillemann and M. Stintz: *J. Aerosol Sci.*, 2009, **40**, 209–217.